N-Doped TiO₂ Nanobelts with Coexposed (001) and (101) Facets and Their Highly Efficient Visible-Light-Driven Photocatalytic Hydrogen Production

Shuchao Sun,[†] Peng Gao,[*,†] Yurong Yang,[†] Piaoping Yang,[*,†] Yujin Chen,[*,‡] and Yanbo Wang[†]

[†]Key Laboratory of Superlight Materials and Surface Technology, Ministry of Education, College of Materials Science and Chemical Engineering, and [‡]College of Science, Harbin Engineering University, Harbin, Heilongjiang 150001, People's Republic of China

S Supporting Information

ABSTRACT: To narrow the band gap (3.2 eV) of TiO₂ and extend its practical applicability under sunlight, the doping with nonmetal elements has been used to tune TiO₂ electronic structure. However, the doping also brings new recombination centers among the photoinduced charge carriers, which results in a quantum efficiency loss accordingly. It has been proved that the {101} facets of anatase TiO₂ are beneficial to generating and transmitting more reductive electrons to promote the H₂-evolution in the photoreduction reaction, and the {001} facets exhibit a higher photoreactivity to accelerate the reaction involved of photogenerated hole. Thus, it was considered by us that using the surface heterojunction composed of both {001} and {101} facets may depress the disadvantage of N doping. Fortunately, we successfully synthesized anatase N-doped TiO₂ nanobelts with a surface heterojunction of coexposed (101) and (001) facets. As expected, it realized the charge pairs' spatial separation and showed higher photocatalytic activity under a visible-light ray: a hydrogen generation rate of 670 μmol h^{-1} g^{-1} (much higher than others reported previously in literature of N-doped TiO₂ nanobelts).

KEYWORDS: hydrogen, surface heterojunction, surface chemistry, photocatalyst, TiO₂
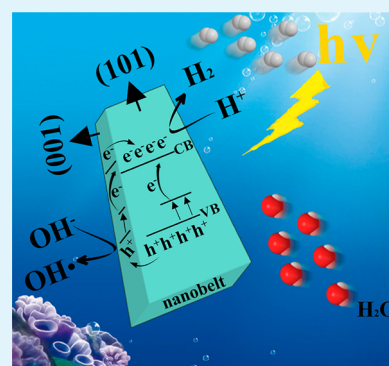
1. INTRODUCTION

The energy poverty induced by the large amount of combustible fossil burning has resulted in an ambitious search for the alternative energy recourses, which are both renewable and environmentally friendly.[1] Since the phenomenon of water generating hydrogen on a TiO₂ photoanode was found in the 1970s,[2] it has drawn great attention on account of its promising applications.[3−5] However, as a typical wide band gap semiconductor (3.2 eV), it has a high recombination rate of photoinduced electron and hole pairs, and its primary absorbance in UV spectrum range also gravely stunts its practical applications under the sunlight.[6] Doping with nonmetal element has been demonstrated as a feasible means to solve the above two problems.[7] However, the doping also brings new recombination centers among the photoinduced charge carriers, which results in the quantum efficiency loss caused by the charge pair recombination accordingly.[8]

According to the past work, it has been proved that the surface heterojunction structure composed of various facets,[9] which have different transmission properties and reactivity for electrons and holes, is conducive to improving the charge pairs separation.[10,11] In anatase TiO₂ crystal, the {101} facets with higher thermodynamic stability often generate and transmit more reductive electrons in hydrogen evolution from the photoreduction reaction.[12,13] Li et al. have synthesized N-doped TiO₂ nanocatalyst with mainly exposed (101) facets, which has a hydrogen production rate of 14.75 μmol h^{-1} g^{-1}.[14]

Differently, TiO₂ nanostructures containing {001} facets exhibited a high photoreactivity to accelerate the photogeneration of holes,[15,16] as shown in Figure 1a. Moreover, N-
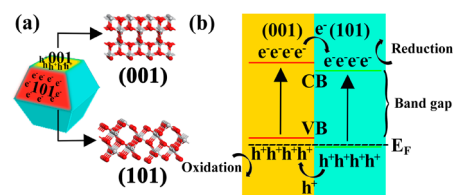

Figure 1. (a) Thermodynamically stable anatase TiO₂ under equilibrium conditions and schematic of atomic structure of (001) and (101) facets. (b) (001) and (101) surface heterojunction.

doped TiO₂ nanocatalyst with mainly exposed (001) facets has a hydrogen production rate of 211 μmol h^{-1} g^{-1} under the visible light.[17] It is seen that N-doped TiO₂ with a single exposed facet presents a low H₂-production rate. Therefore, the surface heterojunction composed of both {101} and {001} facets has been proposed, and it should be more effective to separate the charge pairs (see Figure 1b).[18,19] As illustrated, the Fermi level of {001} approaches the top of {101} surface in the
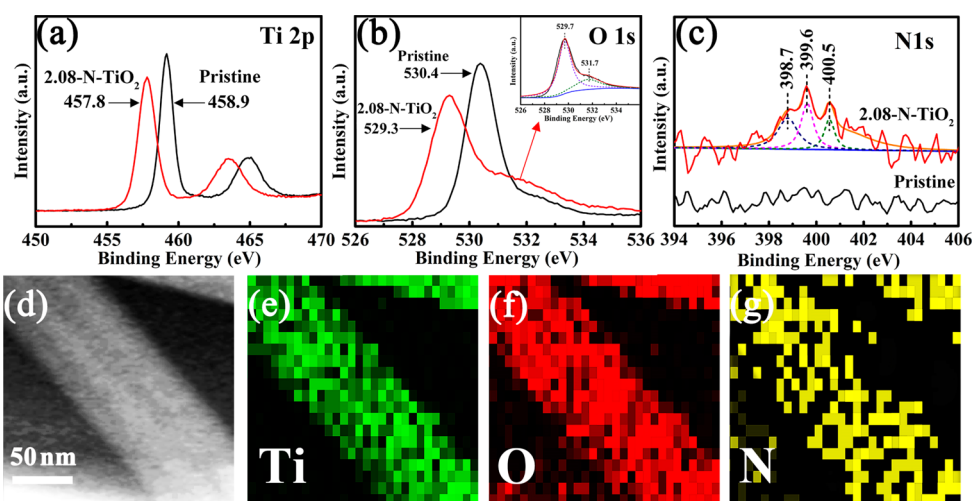
Figure 2. (a–c) XPS spectra of Ti 2p, O 1s, S 2p of 2.08-N-doped TiO_2 nanobelt, respectively; (d–g) TEM images of 2.08-N-doped TiO_2 nanobelt and its corresponding EDS element mapping of Ti, O, and N elements.

valence band.[9] Because of its contact with {101} and {001} facets, the Fermi levels of both of the above facets should be equal. Consequently, it is hardly amazing that the surface heterojunction fabricated of both {101} and {001} (as shown in Figure 1b)[20] favors both separation and transfer of the carriers. In addition, this structure would also narrow the bandgap of TiO_2, favoring the visible light absorbed.

On the basis of the above comprehensive analysis, herein we prepared a serial of N-doped TiO_2 nanobelts with coexposed (001) and (101) facets in surfaces, which are 90 nm wide, 15 nm thick, and 7 μm long. The unique shape of nanobelts provides the well-defined nanostructures with both (101) facet and (001) facet exposed surfaces. As expected, these N-doped TiO_2 nanobelts exhibit a highest hydrogen production rate of 670 μmol h^{-1} g^{-1}, which is much higher than others reported previously in the literature of conventional TiO_2 nanobelts (only several μmol h^{-1} g^{-1}).[16,21]

2. EXPERIMENTAL SECTION

Synthesis of N-Doped TiO_2 Nanobelts. TiO_2 nanobelt precursors were synthesized according to the literature.[36] 0.2 g of TiO_2 precursor was dispersed into 8 mL of deionized water and 12 mL of ethanol in a 50 mL glass beaker. After that, an appropriate amount of ammonium hydroxide was added under stirring. After 2 h, the mixture was transferred into a 50 mL Teflon autoclave and maintained at 180 °C for 12 h. After that, the sample was cooled to room temperature and collected. The as-obtained product was heated to 500 °C for 2 h. The samples of N-doped TiO_2 nanobelt were marked as *n*-N-TiO_2.

Characterization. Powder X-ray diffraction (XRD) data were collected by a D/max-rA X-ray diffractometer (Japan Rigaku) with graphite monochromatized Cu Kα (α = 1.54178 Å). X-ray photoelectron spectroscopy (XPS) measurements were done on an ESCALab220i-XL electron spectrometer and were corrected by a C 1s at 285.0 eV. Scanning electron microscopy (SEM) examinations were conducted on a JEOL-5600LV equipment with a 20 kV accelerating voltage. Transmission electron microscopy (TEM) and the high-resolution transmission electron microscopic (HRTEM) images of N-doped TiO_2 nanobelts were obtained by a JEOL HRTEM equipment. The Brunauer–Emmett–Teller (BET) surface areas of the samples were obtained on the basis of nitrogen adsorption in a Micromeritics ASAP 2020. Diffuse reflectance UV–vis spectra measurements of the samples were proceeded by a UV2550, using BaSO$_4$ as a reflectance standard. The room-temperature photoluminescence (PL) spectra were collected by a spectrophotometer of Jobin Yvon Fluorolog 3-221

using a Xe lamp (450 W, 380 nm) as excitation source. The photocurrent measurements were recorded on a semiconductor characterization system (Keithley 4200 SCS) with a Lakeshore probe station and a xenon lamp (300 W, λ > 400 nm).

Photocatalytic H$_2$-Production from Water Splitting. The photocatalytic water splitting was performed in a 500 mL Pyrex reaction cell. A 300 W xenon arc lamp with a filter (UVCUT400: 400–800 nm) was applied as a visible light source to induce the photocatalytic reaction. The photocatalytic H$_2$-evolution from water splitting was measured using an CEL-SPH2N equipment. In a typical photocatalytic experiment, 0.1 g of catalyst sample was placed into 100 mL of a methanol solution (20 mL of methanol) in the reaction cell. The 0.5 wt % Pt was conducted by directly dissolving H$_2$PtCl$_6$ in the aforementioned 100 mL of mixed solution as cocatalyst.

3. RESULTS AND DISCUSSION

The chemical composition measurements based on XPS analysis of the above as-obtained samples were carried out first, as shown in Figure 2a–c. As expected, similar peaks due to species containing Ti, O, and N in all products are presented in the wide scan XPS spectra. As shown in Figure 2a, two peaks at binding energies of 458.6 and 464.2 eV due to Ti 2$P_{3/2}$ and 2$P_{1/2}$, respectively, are found for TiO_2 samples. In its O 1s spectrum (Figure 2b, inset), an obvious peak at 529.6 eV and a shoulder peak at 531.7 eV are detected, which are due to the lattice oxygen in TiO_2[17] and physisorbed water,[22] respectively. After doping with N, the binding energies of Ti 2$P_{3/2}$ shift from 458.9 to 457.8 eV and the O 1s peaks from 530.4 to 529.3 eV, respectively, as listed in Table 1. In addition, a DFT calculation has pointed out that the doping of nitrogen resulted in a decrease of the energy cost to the formation of oxygen vacancies.[23]

Figure 2c shows the N 1s spectra of 2.08-N-doped TiO_2 nanobelts with a broad peak ranging from 398 to 401 eV, which is a characteristic peak of the as-doped nitrogen.[24,25] The peak at 398.7 eV (peak 1) is attributed to replacing O with N (N–Ti–O).[26] The peaks at 399.6 eV (peak 2) and 400.5 eV (peak 3) belong to the Ti–O–N bonding[27] and the nitrogen species constrained on the surface (essentially adsorbed NO$_x$).[28] It would improve the binding energy of the N 1s level. According to the XPS analysis, the contents of nitrogen in TiO_2 matrixes obtained by us are 0.53, 0.75, 0.91, 1.32, 1.68, and 2.08 at. %, respectively. Besides the XPS results, energy-dispersive X-ray spectroscopy (EDS) mapping is also performed to confirm its

Table 1. Nitrogen Content and XPS Peak Positions of the As-Obtained Nanobelts

sample	N content (at. %)	Ti 2P$_{3/2}$ (eV)	O 1s (eV)
pristine		458.9	530.4
0.53-N-TiO$_2$	0.53	458.6	530.0
0.75-N-TiO$_2$	0.75	458.4	529.7
0.91-N-TiO$_2$	0.91	458.2	529.5
1.32-N-TiO$_2$	1.32	458.1	529.4
1.68-N-TiO$_2$	1.68	457.8	529.3
2.08-N-TiO$_2$	2.08	457.8	529.3

element distribution. As shown in Figure 2d−g, it further confirms the large-scale existence of the Ti, O, and N elements, which agrees well with the XPS analysis.

Figure 2c shows the N 1s spectra of 2.08-N-doped TiO$_2$ nanobelts with a broad peak ranging from 398 to 401 eV, which is a characteristic peak of the as-doped nitrogen.[24,25] The peak at 398.7 eV (peak 1) is attributed to replacing O with N (N−Ti−O).[26] Also, the peaks at 399.6 eV (peak 2) and 400.5 eV (peak 3) belong to the Ti−O−N bonding[27] and the nitrogen species constrained on the surface (essentially adsorbed NO$_x$).[28] It would improve the binding energy of the N 1s level. According to the XPS analysis, the contents of nitrogen in TiO$_2$ matrixes obtained by us are 0.53, 0.75, 0.91, 1.32, 1.68, and 2.08 at. %, respectively. Besides the XPS results, energy-dispersive X-ray spectroscopy (EDS) mapping is also performed to confirm its element distribution. As shown in Figure 2d−g, it further confirms the large-scale existence of the Ti, O, and N elements, which agrees well with the XPS analysis.

After that, XRD measurements of the desiccative TiO$_2$ powder with different N-doped atomic percentages were conducted. Figure 3a shows the XRD patterns of N-doped
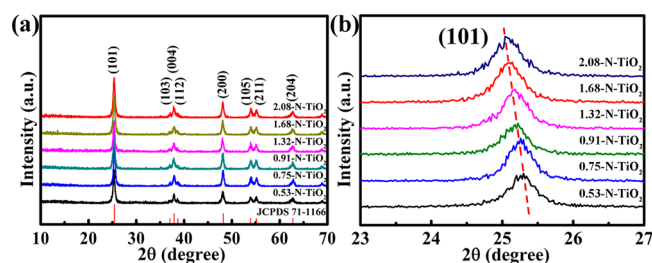

Figure 3. (a) XRD patterns of sample TiO$_2$ nanobelt precursor and N-doped TiO$_2$ with different doping percentage; and (b) enlarged (101) peaks of N-doped TiO$_2$ samples.

TiO$_2$ samples and that of pure anatase TiO$_2$ reported in the literature (JCPDS 71-1166). No peak for nitride is observed, which indicates that nitrogen atoms have been well-dispersed into the TiO$_2$ matrix. This result agrees well with its XPS and EDS mapping results, as shown in Figure 2. Accordingly, the nitrogen doping triggers a broadening effect on the TiO$_2$ XRD peaks. On the basis of the above XPS and XRD analysis, it is unambiguous that with the nitrogen doping, the site of O$^{2−}$ in TiO$_2$ is substituted by a nitrogen cation with a larger atomic radius (O$^{2−}$ = 140 Å and N$^{3−}$ = 171 Å), resulting in the lattice spacing increasing. Representatively, the peaks of the (101) reflection plane of the N-doped TiO$_2$ samples shift to lower diffraction angles relative to that of pure TiO$_2$ (Figure 3b). To further study the effect of the large lattice distortion on recombination center, PL measurements with a same addition amount have been conducted to evaluate the defect

concentration after doping with N element, as shown in Figure S1. It is found that with the increase of N doping amount, their PL intensities decline due to the defects.[29] So the defects coming from the large lattice distortion do not introduce new recombination centers.

The morphologies and microstructures of N-doped TiO$_2$ nanobelts are characterized by SEM, TEM, and HRTEM examinations, as shown in Figure 4. In the SEM images (Figure 4a−c), it can be seen that TiO$_2$ doped by nitrogen are all nanobelts. This characteristic indicates that the N doping does not obviously affect the morphology of TiO$_2$ nanobelt precursor. In addition, the 1D nanostructures with extraordinarily smooth surfaces are up to ca. 7 μm in length. It is clear that the N-doped TiO$_2$ samples have a high orientation growth and a considerably high aspect ratio up to 77.8 (i.e., length divided by wide), which may improve their physicochemical activities. On the basis of the symmetry relations of anatase TiO$_2$ crystals, as shown in Figure 4c, inset, the two exposed planes are (001) and (101), respectively.[30−32] Furthermore, the interfacial angle of 111.8° between the above planes also proves the above result. The corresponding TEM and HRTEM images of 2.08 N-doped TiO$_2$ nanobelts are shown in Figure 4d−f. It is seen that the nanoparticles are 90 nm wide and ca. 15 nm thick. All of these characteristics indicate that the TiO$_2$ nanobelts have two outstandingly exposed (001) and (101) facets, which make up a surface heterojunction.

Their UV−visible diffuse reflectance spectrum measurements further confirm the above observation, as shown in Figure 5a. With increasing nitrogen content, the curves show an enhanced absorbance in the visible light. It can be seen that, as compared to the pure TiO$_2$, the N-doped TiO$_2$ samples exhibit relatively stronger absorption, which is caused by N doping. Therefore, the N-doping of TiO$_2$ nanobelts further enhances the visible light absorption. Moreover, according to the XPS tests, the N−Ti−O and Ti−O−N bonds formed in the samples could introduce some shallow trap states at the surface or undersurface of TiO$_2$. It is deduced that the decrease of bandgap increases the light absorption, and electrons through absorbing a lower photon energy in the valence band more easily jump to the conduction band. Thereby, the as-displayed optical results of N-TiO$_2$ imply more efficient processes for visible-light photocatalytic water splitting for H$_2$ generation once they are used as photocatalysts.

The large specific surface area of catalyzer is admitted to contain more reactive sites to promote the catalysis reactions. So the surface area of our N-doped TiO$_2$ samples is examined first by a N$_2$ adsorption−desorption measurement. Figure S2 shows that typical Langmuir III type characteristic isotherms followed by hysteresis loops are obtained in all of the specimens. The pressure range of the BET analysis is performed over the range 0.06 < $P/P°$ < 0.3, which is on the basis of the multipoint BET method, as shown in Figure S3. The specific surface areas of the 0.53-N-TiO$_2$, 1.32-N-TiO$_2$, and 2.08-N-TiO$_2$ nanobelts were 30, 32, and 34 m^2 g$^{−1}$, respectively. So their surface areas are not the main factor for their different photocatalytic abilities.

The photocatalytic activities for water splitting are also measured. Figure 5b shows the H$_2$ evolution with different reaction times over the TiO$_2$ nanobelt precursor and N-doped TiO$_2$ samples under visible light (400 nm < λ < 800 nm). It is found that the sample of 2.08-N-TiO$_2$ nanobelts steadily produces hydrogen at a 670 μmol h$^{−1}$ g$^{−1}$ rate, much higher than the values of other N-doped TiO$_2$ nanobelts with a single
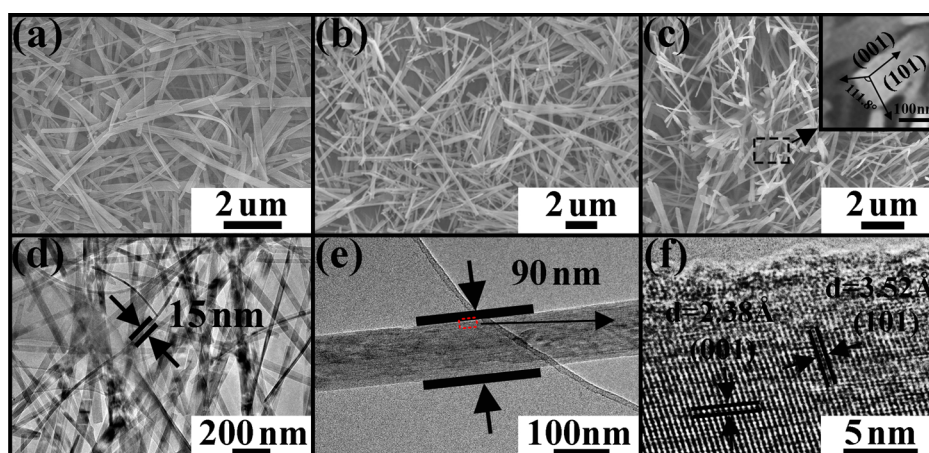
Figure 4. SEM images of (a) 0.53-N-TiO$_2$, (b) 1.32-N-TiO$_2$, and (c) 2.08-N-TiO$_2$; (d,e) TEM images and (f) HRTEM image of 2.08-N-TiO$_2$ nanobelts.
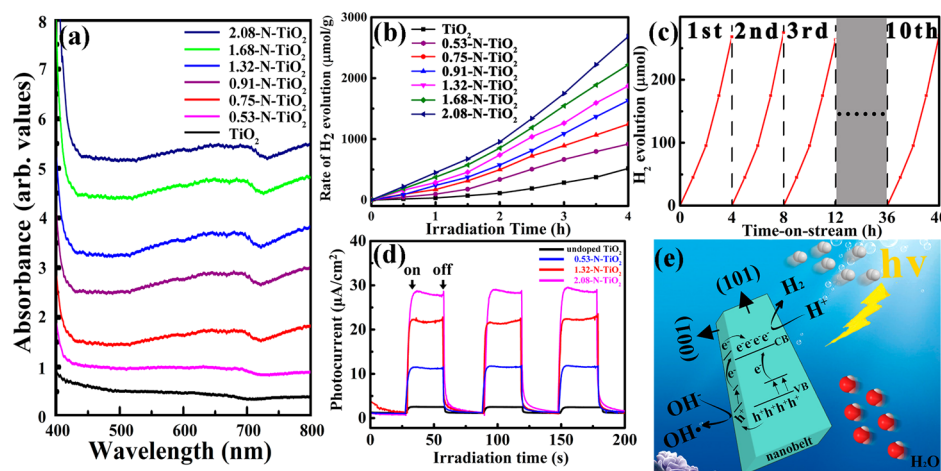

Figure 5. (a) UV−vis diffuse reflectance (DR) spectra of the samples. (b) H$_2$ production rates of the products. (c) Cycling stability results of photocatalytic H$_2$ production over 2.08-N-TiO$_2$ sample. (d) Photocurrent responses under illumination ($\lambda > 400$ nm) of undoped TiO$_2$ nanobelts, 0.53-N-TiO$_2$ nanobelts, 1.32-N-TiO$_2$ nanobelts, and 2.08-N-TiO$_2$ nanobelts. (e) Diagram of the charge shift process in N-doped TiO$_2$ nanobelt.

facet exposed.[16,17] In addition, the hydrogen evolution on different amounts of 2.08-N-TiO$_2$ nanobelt photocatalyst is further investigated, as shown in Figure S4. The hydrogen evolution rate of 2.08-N-TiO$_2$ rapidly increases from 4.9 μmol h^{-1} with 0.01 g of sample to the maximum rate of 67 μmol h^{-1} with 0.1 g of sample, and then decreases to 60.5 μmol h^{-1} with 0.2 g of sample. With increasing content of photocatalyst, the absorbed photons will reach a saturation state and cut off the continually injected photons.[33] Besides the high H$_2$ production rate, the 2.08-N-TiO$_2$ nanobelt also displays a satisfactory stability. As shown in Figure 5c, no obvious decrease for hydrogen production is detected in our cycling stability tests.

The photocurrent responses of our samples have also been conducted under visible light. As shown in Figure 5d, it is clear that the TiO$_2$ nanobelts with an increasing N content have remarkably enhanced photocurrents under visible light, which is consistent with their photocatalytic performances: 2.08-N-TiO$_2$ > 1.32-N-TiO$_2$ > 0.53-N-TiO$_2$ > undoped TiO$_2$.

Herein, the higher hydrogen evolution rate is mainly attributed to the following factors. First, the nanobelt structure provides a more optimized and stable geometry. Also, when the nitrogen doping atomic percentage is up to 2.08 at. %, the bandgap is narrowed to 2.96 eV. More importantly, the as-

obtained nanobelts expose two dominant surfaces of (101) and (001) facets and exhibit enhanced photocatalytic activities, which should be due to the following two respects. On one hand, the surface heterojunction induces an electrostatic force. Once the samples are under the light, its valence band electrons are excited to the conduction band level. The electrons in (001) will be attracted immediately to (101) due to the electrostatic force and rapidly pass through them to reach the surface. As a direct result, the (101) facet of the nanobelts has a large number of photogenerated electrons, and the electrons ultimately transfer to the active reaction sites to combine with H$^+$ to release H$_2$. On the other hand, due to the existence of surface heterojunction, the holes will be attracted immediately from (101) to (001). It has been indicated that the (001) surfaces have a better capability of promoting the holes reacted with OH$^-$ to form hydroxyl radicals (OH$^•$).[34,35] In addition, the nanobelt structure exposing two dominant surfaces of (101) and (001) facets not only promotes water molecule disintegration but also improves the abilities of the charge pairs' spatial separation. Thereby, the as-obtained N-doped TiO$_2$ nanobelts with coexposed (001) and (101) facets have enhanced hydrogen evolution activities, as proposed in Figure 5e.

4. CONCLUSION

Herein, N-doped TiO_2 nanobelts with surface heterojunctions composed of coexposed (001) and (101) facets have exhibited a high efficiency (670 μmol h^{-1} g^{-1}) for photocatalytic H_2 production from water splitting under visible-light irradiation. In the catalytic process, the surface heterojunction not only promotes the water molecule disintegration but also improves the abilities of the charge pairs' spatial separation to effectively inhibit the recombination of the electron−hole pairs. The significantly improved photocatalytic activity of N-doped TiO_2 nanobelt may enlighten the design of other robust semiconductor photocatalysts in this field.

■ ASSOCIATED CONTENT

Ⓢ Supporting Information

The Supporting Information is available free of charge on the ACS Publications website at DOI: 10.1021/acsami.6b05244.

(1) Photoluminescence spectra of undoped TiO_2 nanobelts, 0.53-N-TiO_2 nanobelts, 1.32-N-TiO_2 nanobelts, and 2.08-N-TiO_2 nanobelts; (2) nitrogen adsorption−desorption isotherms of TiO_2 nanobelts: (1) 0.53-N-TiO_2 (black plot), (2) 1.32-N-TiO_2 (red plot), and (3) 2.08-N-TiO_2 (blue plot); (3) multipoint BET curves of 0.53-N-TiO_2 nanobelts, 1.32-N-TiO_2 nanobelts, and 2.08-N-TiO_2 nanobelts; and (4) photocatalytic H_2 production activities of the 2.08-N-TiO_2 nanobelts with different addition amounts (PDF)

■ AUTHOR INFORMATION

Corresponding Authors

*E-mail: gaopeng@hrbeu.edu.cn.
*E-mail: yangpiaoping@hrbeu.edu.cn.
*E-mail: chenyujin@hrbeu.edu.cn.

Notes

The authors declare no competing financial interest.

■ ACKNOWLEDGMENTS

■ REFERENCES

(1) Cortright, R. D.; Davda, R. R.; Dumesic, J. A. Hydrogen from Catalytic Reforming of Biomass-derived Hydrocarbons in Liquid Water. *Nature* **2002**, *418*, 964−967.

(2) Fujishima, A.; Honda, K. Electrochemical Photolysis of Water at a Semiconductor Electrode. *Nature* **1972**, *238*, 37−38.

(3) Hoffmann, M. R.; Martin, S. T.; Choi, W.; Bahnemann, D. W. Environmental Applications of Semiconductor Photocatalysis. *Chem. Rev.* **1995**, *95*, 69−96.

(4) Thompson, L.; Yates, J. Surface Science Studies of the Photoactivation of TiO_2-new Photochemical Processes. *Chem. Rev.* **2006**, *106*, 4428−4453.

(5) Ravelli, D.; Dondi, D.; Fagnoni, M.; Albini, A. Photocatalysis. A Multi-faceted Concept for Green Chemistry. *Chem. Soc. Rev.* **2009**, *38*, 1999−2011.

(6) Chen, X.; Mao, S. S. Titanium Dioxide Nanomaterials: Synthesis, Properties, Modifications and Application. *Chem. Rev.* **2007**, *107*, 2891−2959.

(7) Li, L.; Yan, J.; Wang, T.; Zhao, Z.; Zhang, J.; Gong, J.; Guan, N. Sub-10 nm Rutile Titanium Dioxide Nanoparticles for Efficient Visible-light-driven Photocatalytic Hydrogen Production. *Nat. Commun.* **2015**, *6*, 5881−5891.

(8) Naldoni, A.; Allieta, M.; Santangelo, S.; Marelli, M.; Fabbri, F.; Cappelli, S.; Bianchi, C. L.; Psaro, R.; Santo, V. D. Effect of Nature and Location of Defects on Bandgap Narrowing in Black TiO_2 Nanoparticles. *J. Am. Chem. Soc.* **2012**, *134*, 7600−7603.

(9) Yu, J.; Low, J.; Xiao, W.; Zhou, P.; Jaroniec, M. Enhanced Photocatalytic CO_2-Reduction Activity of Anatase TiO_2 by Coexposed {001} and {101} Facets. *J. Am. Chem. Soc.* **2014**, *136*, 8839−8842.

(10) Zhang, J.; Xu, Q.; Feng, Z.; Li, M.; Li, C. Importance of the Relationship Between Surface Phases and Photocatalytic Activity of TiO_2. *Angew. Chem., Int. Ed.* **2008**, *47*, 1766−1769.

(11) Murdoch, M.; Waterhouse, G. I. N.; Nadeem, M. A.; Metson, J. B.; Keane, M. A.; Howe, R. F.; Llorca, J.; Idriss, H. The Effect of Gold Loading and Particle Size on Photocatalytic Hydrogen Production from Ethanol over Au/TiO_2 Nanoparticles. *Nat. Chem.* **2011**, *3*, 489−492.

(12) Pan, J.; Liu, G.; Lu, G. Q.; Cheng, H. M. On the True Photoreactivity Order of {001}, {010}, and {101} Facets of Anatase TiO_2 Crystals. *Angew. Chem., Int. Ed.* **2011**, *50*, 2133−2137.

(13) Wu, N.; Wang, J.; Tafen, D. N.; Wang, H.; Zheng, J. G.; Lewis, J. P.; Liu, X.; Leonard, S. S.; Manivannan, A. Shape-Enhanced Photocatalytic Activity of Single-Crystalline Anatase TiO_2 (101) Nanobelts. *J. Am. Chem. Soc.* **2010**, *132*, 6679−6685.

(14) Li, Y.; Ma, G.; Peng, S.; Lu, G.; Li, S. Boron and Nitrogen co-doped Titania with Enhanced Visible-light Photocatalytic Activity for Hydrogen Evolution. *Appl. Surf. Sci.* **2008**, *254*, 6831−6836.

(15) Bai, Y.; Mora-Seró, I.; Angelis, F. D.; Bisquert, J.; Wang, P. Titanium Dioxide Nanomaterials for Photovoltaic Applications. *Chem. Rev.* **2014**, *114*, 10095−10130.

(16) Li, C.; Koenigsmann, C.; Ding, W.; Rudshteyn, B.; Yang, K. R.; Regan, K. P.; Konezny, S. J.; Batista, V. S.; Brudvig, G. W.; Schmuttenmaer, C. A.; Kim, J. Facet-Dependent Photoelectrochemical Performance of TiO_2 Nanostructures: An Experimental and Computational Study. *J. Am. Chem. Soc.* **2015**, *137*, 1520−1529.

(17) Xiang, Q.; Yu, J.; Wang, W.; Jaroniec, M. Nitrogen Self-doped Nanosized TiO_2 Sheets with Exposed {001} Facets for Enhanced Visible-light Photocatalytic Activity. *Chem. Commun.* **2011**, *47*, 6906−6908.

(18) Liu, X.; Dong, G.; Li, S.; Lu, G.; Bi, Y. Direct Observation of Charge Separation on Anatase TiO_2 Crystals with Selectively Etched {001} Facets. *J. Am. Chem. Soc.* **2016**, *138*, 2917−2920.

(19) Maisano, M.; Dozzi, M. V.; Coduri, M.; Artiglia, L.; Granozzi, G.; Selli, E. Unraveling the Multiple Effects Originating the Increased Oxidative Photoactivity of {001}-Facet Enriched Anatase TiO_2. *ACS Appl. Mater. Interfaces* **2016**, *8*, 9745−9754.

(20) Liu, L.; Jiang, Y.; Zhao, H.; Chen, J.; Cheng, J.; Yang, K.; Li, Y. Engineering Coexposed {001} and {101} Facets in Oxygen-Deficient TiO_2 Nanocrystals for Enhanced CO_2 Photoreduction under Visible Light. *ACS Catal.* **2016**, *6*, 1097−1108.

(21) Liu, G.; Yang, H. G.; Wang, X.; Cheng, L.; Pan, J.; Lu, G. Q.; Cheng, H. Visible Light Responsive Nitrogen Doped Anatase TiO_2 Sheets with Dominant {001} Facets Derived from TiN. *J. Am. Chem. Soc.* **2009**, *131*, 12868−12869.

(22) Wang, J.; Tafen, D. N.; Lewis, J. P.; Hong, Z.; Manivannan, A.; Zhi, M.; Li, M.; Wu, N. Origin of Photocatalytic Activity of Nitrogen-Doped TiO_2 Nanobelts. *J. Am. Chem. Soc.* **2009**, *131*, 12290−12297.

(23) Ketteler, G.; Yamamoto, S.; Bluhm, H.; Andersson, K.; Starr, D. E.; Ogletree, D. F.; Ogasawara, H.; Nilsson, A.; Salmeron, M. The Nature of Water Nucleation Sites on TiO_2 (110) Surfaces Revealed by Ambient Pressure X-ray Photoelectron Spectroscopy. *J. Phys. Chem. C* **2007**, *111*, 8278−8282.

(24) Sathish, M.; Viswanathan, B.; Viswanath, R. P.; Gopinath, C. S. Synthesis, Characterization, Electronic Structure, and Photocatalytic

Activity of Nitrogen-Doped TiO$_2$ Nanocatalyst. *Chem. Mater.* **2005**, *17*, 6349−6353.

(25) Asahi, R.; Morikawa, T.; Ohwaki, T.; Aoki, K.; Taga, Y. Visible-Light Photocatalysis in Nitrogen-Doped Titanium Oxides. *Science* **2001**, *293*, 269−271.

(26) Burda, C.; Lou, Y.; Chen, X.; Samia, A. C. S.; Stout, J.; Gole, J. L. Enhanced Nitrogen Doping in TiO$_2$ Nanoparticles. *Nano Lett.* **2003**, *3*, 1049−1051.

(27) Gole, J. L.; Stout, J. D.; Burda, C.; Lou, Y.; Chen, X. J. Highly Efficient Formation of Visible Light Tunable TiO$_{2-x}$N$_x$ Photocatalysts and Their Transformation at the Nanoscale. *J. Phys. Chem. B* **2004**, *108*, 1230−1240.

(28) Yan, J.; Wu, G.; Guan, N.; Li, L.; Li, Z.; Cao, X. Understanding the Effect of Surface/Bulk Defects on the Photocatalytic Activity of TiO$_2$: Anatase Versus Rutile. *Phys. Chem. Chem. Phys.* **2013**, *15*, 10978−10988.

(29) Hu, Z.; Xu, L.; Chen, J. Ordered Arrays of N-doped Mesoporous Titania Spheres with High Visible Light Photocatalytic Activity. *Mater. Lett.* **2013**, *106*, 421−424.

(30) Liu, S.; Yu, J.; Jaroniec, M. Tunable Photocatalytic Selectivity of Hollow TiO$_2$ Microspheres Composed of Anatase Polyhedra with Exposed {001} Facets. *J. Am. Chem. Soc.* **2010**, *132*, 11914−11916.

(31) Han, X.; Kuang, Q.; Jin, M.; Xie, Z.; Zheng, L. Synthesis of Titania Nanosheets with a High Percentage of Exposed (001) Facets and Related Photocatalytic Properties. *J. Am. Chem. Soc.* **2009**, *131*, 3152−3153.

(32) Yang, H. G.; Liu, G.; Qiao, S. Z.; Sun, C. H.; Jin, Y. G.; Smith, S. C.; Zou, J.; Cheng, H. M.; Lu, G. Q. Solvothermal Synthesis and Photoreactivity of Anatase TiO$_2$ Nanosheets with Dominant {001} Facets. *J. Am. Chem. Soc.* **2009**, *131*, 4078−4083.

(33) Liu, R.; Zhou, X.; Yang, F.; Yu, Y. Combination Study of DFT Calculation and Experiment for Photocatalytic Properties of S-doped Anatase TiO$_2$. *Appl. Surf. Sci.* **2014**, *319*, 50−59.

(34) Linsebigler, A. L.; Lu, G.; Yates, J. T. Photocatalysis on TiO$_2$ Surfaces: Principles, Mechanisms, and Selected Results. *Chem. Rev.* **1995**, *95*, 735−758.

(35) Peiro, A. M.; Colombo, C.; Doyle, G.; Nelson, J.; Mills, A.; Durrant, J. R. Photochemical Reduction of Oxygen Adsorbed to Nanocrystalline TiO$_2$ Films: A Transient Absorption and Oxygen Scavenging Study of Different TiO$_2$ Preparations. *J. Phys. Chem. B* **2006**, *110*, 23255−23263.

(36) Gao, P.; Bao, D.; Wang, Y.; Chen, Y.; Wang, L.; Yang, S.; Chen, G.; Li, G.; Sun, Y.; Qin, W. Epitaxial Growth Route to Crystalline TiO$_2$ Nanobelts with Optimizable Electrochemical Performance. *ACS Appl. Mater. Interfaces* **2013**, *5*, 368−373.